

Dipole-induced processes in HeH^+ produced by an excited $\text{Li}(2p)$ neighbor: From charge transfer to virtual photon dissociation, and formation of LiH and LiHe

R. Cabrera-Trujillo ^{1,*}, O. Vendrell ² and L. S. Cederbaum²

¹*Instituto de Ciencias Físicas, Universidad Nacional Autónoma de México, Av. Universidad S/N, Col. Chamilpa, Cuernavaca, Morelos 62210, Mexico*

²*Theoretische Chemie, Physikalisch-Chemisches Institut, Universität Heidelberg, INF 229, 69120 Heidelberg, Germany*



(Received 17 November 2021; accepted 14 April 2022; published 2 May 2022)

Dipole interaction between neighbor systems is of importance in the behavior of atoms and molecules as it produces distortion in the electronic structure of the system. In this work, we study the dipole processes in a HeH^+ molecule induced by an initially excited lithium atom placed at an R_0 distance from the center of mass of the molecule. The electronic and nuclear degrees of freedom are treated by the electron-nuclear dynamics approach as it allows a time-dependent description of the electronic and nuclear dynamics. The energy transferred from the neighbor excited lithium atom to the HeH^+ molecule is distributed into several channels depending on the initial vibrational state of the HeH^+ and initial R_0 separation. We find that several processes are induced by the dipole interaction. Among these, we find that the charge-transfer channel from the Li onto the ionic molecule HeH^+ is the dominant outcome. Also, we find that a virtual photon dissociation process takes place via a dipole interaction that induces nuclear motion of the molecule through an electronic relaxation of the initial lithium $2p$ electron to the $2s$ state or to the $1s$ state of the He or H atom of the neighbor system, as well as vibrational intermolecular energy transfer. We report dissociation of the HeH^+ molecule followed by chemical rearrangement leading to the formation of LiH and LiHe molecules and their respective charged ions. We find that deexcitation occurs on femtosecond while the molecular dissociation on picosecond time scales. Consequently, the dipole interaction between neighbors induces a richer dynamics.

DOI: [10.1103/PhysRevA.105.053104](https://doi.org/10.1103/PhysRevA.105.053104)

I. INTRODUCTION

The dipole interaction of atoms with a neighbor system is known to cause distortions in the atom or molecule electronic structure with effects in the broadening of spectral lines as well as in the decay process. For example, the dipole-dipole interaction is responsible for the dipole blockade and collective excitations observed in Rydberg atoms [1]. Also, the dipole interaction involves interatomic-molecular energy-transfer processes between an atom or molecule and its neighbors. If the energy transferred is electronic and between bound electronic states of the molecule and one of its molecular neighbors, the process is referred to as Förster resonance energy transfer (FRET) [2]. FRET is only possible if nuclear motion takes place due to energy conservation and this leads to a timescale of picoseconds or longer in the dynamics [3]. Another highly efficient dipole-induced electronic energy-transfer mechanism is the interatomic Coulombic decay (ICD) [4]. The ICD process becomes operative once the excess energy suffices to ionize the neighbor and hence energy conservation is fulfilled without the need for nuclear motion. In the ICD process, the excited species as well as the neighbors can be atoms or molecules and the timescale involved is in the femtosecond regime. Applications of ICD appear in extreme systems like the He dimer [5], ICD after Auger and

resonant Auger processes [6–10], and ICD in quantum dots and quantum wells [11–14].

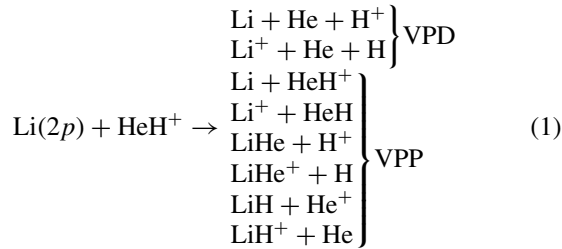
Recently, it has been predicted that the dipole interaction induces vibrational energy transfer from electronic degrees of freedom [15] leading to molecular dissociation induced by neighbor deexcitation via virtual photons. Traditionally molecular dissociation is achieved through the absorption of light, called photodissociation. The understanding of bond breaking in the photodissociation process is of relevance in chemistry, molecular science, and astrophysics, where it has attracted a vast amount of research [16,17].

There exist several theoretical approaches to study dipole-induced interaction processes. One approach consists in calculating transition rates using *ab initio* calculation of interatomic decay rates by a combination of the Fano ansatz, Green's-function methods, the Stieltjes imaging technique [18], and extensions thereof like the Fano-Stieltjes method applied to Lanczos pseudospectra [19]. Another approach relies on the Hamiltonian continued into the complex energy plane [20–24]. The decaying states become resonances with complex energies, where the imaginary part is related to the inverse lifetime. In the above methods, the transition rates are calculated at fixed values of the interatomic distances and the nuclear dynamics of the process is calculated afterwards using the resulting complex potential-energy surfaces [25–27]. In the case of photodissociation, there is a wealth of literature that can be traced back to the work of Shapiro [28] and Balint-Kurti [29].

*Corresponding author: trujillo@icf.unam.mx

In general, a molecule undergoing photodissociation is not isolated and one may ask what the effect is of a neighbor. Motivated by the former work of Ref. [30], we study the case when the molecule and its neighbor are well separated and unbounded such that if the photon is absorbed by the molecule, the photodissociation process is only little affected. We shall show, however, that if the impinging photon is absorbed by the neighbor atom, the molecule can still undergo dissociation. This process is called virtual photon dissociation (VPD) [30]. Here, we propose to study the dipole-induced processes of the HeH^+ molecular ion in the neighborhood of an excited lithium atom. There has been much experimental and theoretical interest in HeH^+ , which is the simplest heteronuclear two-electron system made of the two most abundant elements in the universe (see, for instance, Ref. [31] and references therein as well as [32], particularly in the study of photodissociation).

The possible final channels induced by the dipole interaction at hand are



each of them with a probability and kinetic energy (KE). The first two channels leading to dissociation are of the VPD type and all the other processes are also the result of a virtual photon and are called virtual photon processes (VPP).

In order to study the dipole-induced process from first principles, we propose to use a theoretical approach based on an *ab initio* time-dependent solution of the Schrödinger equation that incorporates electronic and nuclear coupling to account for the molecular dissociation, rearrangement, and electron transfer processes. Our approach is called electron-nuclear dynamics (END) [33]. The current version of END is limited to a single determinant. This results in the appearance of partial Mulliken charges and associated Coulomb forces, and these can have an effect on the fragmentation dynamics of the HeH^+ molecule under consideration besides induced-dipole interactions. Nonetheless, the END approach provides a well-defined and improvable *ab initio* model for electron-nuclear dynamics. We benchmark it on a dipole-induced process, e.g., VPD, a challenging mechanism dominated by electron-nuclear correlations, while presenting the advantages and limitations of this approach in this low-energy regime. END has been applied to atomic and molecular processes, such as collisions [34–36], electron charge exchange [36–38], molecular fragmentation [39,40], energy-loss (stopping power) process [35,41,42], and interatomic Coulomb decay [43], with excellent results.

The layout of our work is the following. In Sec. II A, we present the dipole-induced VPD physical assumptions, while in Sec. II B a summary of the electron-nuclear dynamics approach, as implemented for the study of the VPD, is provided. In Sec. II C, we give the computational details for the $\text{Li} + \text{HeH}^+$ dynamics, as within the END description. Our results and discussion are presented in Sec. III starting with

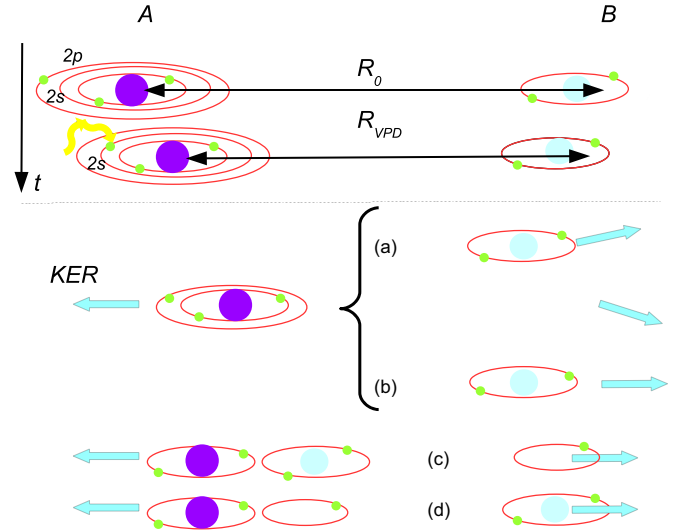


FIG. 1. Sketch of the virtual-photon dissociation process occurring for a diatomic molecule and an excited atom as a neighbor. The systems A and B are initially separated by a distance R_0 with the molecule B being the HeH^+ molecule and A being the excited lithium atom (neighbor). As time passes by (vertical arrow, upper part), the dipole interaction causes them to attract and the VPD occurs at a critical distance R_{VPD} . The possible processes are (a) dissociation, (b) Coulomb repulsion with a final kinetic energy (KE) with or without charge exchange, (c) chemical rearrangement into LiHe^+ or LiHe with a final KE, and (d) chemical rearrangement into LiH^+ or LiH with a final KE. See text for discussion.

the dipole-induced process by means of the study of the trajectories and final electron charge distribution, the dissociation, the chemical rearrangement, and the vibrational internuclear energy transfer. We conclude this section with a study of the kinetic energy of the fragments and the effect of the vibrational temperature on the VPD. Finally, our conclusions are given in Sec. IV.

II. THEORY

A. Virtual photon dissociation

As the details of dipole-induced VPD have been reported previously in Ref. [30], here we provide a summary of the main physical assumptions.

Let us consider two atomic or molecular systems denoted as A and B, separated by a distance R_0 , as depicted in Fig. 1. The rate of the VPD relaxation process is determined by Fermi's golden rule by means of a dipole interaction between system A and its neighbor B

$$\Gamma = \frac{4\pi}{3R_0^6} \sum_f |\mathbf{D}_{i,f}^A|^2 |\mathbf{D}_{i,f}^B|^2. \quad (2)$$

Here $\mathbf{D}_{i,f}^A = \langle \phi_i^A | \mathbf{D}^A | \phi_f^A \rangle$ is the transition dipole moment of system A and with a similar expression for system B from the initial state i to a final state j , where ϕ_i^k is the atomic or molecular wave function of system $k \in \{A, B\}$. Equation (2) implies that systems with large allowed transition dipole moments have a large VPD rate.

The VPD process can be interpreted as follows. The neighbor system A achieves an excess energy through excitation by the absorption of a photon or by collisions with another particle. This excess energy may be in the form of an electronic excitation that can either be carried away from the A subsystem by emission of a photon or transferred via Coulomb forces to the B subsystem in which a dissociation or chemical rearrangement is induced afterwards. When possible energetically, the latter nonradiative mechanism of deexcitation is extremely efficient in comparison to the competing photon emission [15]. Of particular importance is the case when one of the systems is a molecular target. The molecule undergoes dissociation by a virtual photon emitted from the neighbor, but this process induces a much richer dynamics, e.g., charge exchange or chemical rearrangement might occur. In this context, charge transfer is a deexcitation into any of the atomic orbitals that form the system induced by a virtual photon. The process depicted here assumes two static systems A and B separated initially by a distance R_0 . In order to have a detailed time evolution of the dissociation or chemical rearrangement process induced by the interaction, we need to solve the time-dependent Schrödinger equation with coupled electron-nuclear dynamics to gain an insight of the dynamics.

B. Electron-nuclear dynamics approach

The simplest and current level of the END theory employs a coupled wave function $|\psi\rangle = |z, \mathbf{R}, \mathbf{P}\rangle |\mathbf{R}, \mathbf{P}\rangle$, where $|\mathbf{R}, \mathbf{P}\rangle$ is the nuclear wave function with \mathbf{R}_k and \mathbf{P}_k denoting the average position and momentum of the k th nucleus, respectively. Here $|z, \mathbf{R}, \mathbf{P}\rangle$ is a complex, spin unrestricted, electronic single determinantal wave function, which is built from dynamical molecular spin orbitals

$$\chi_i = \phi_i + \sum_{j=N+1}^K \phi_j z_{ji}, \quad (3)$$

with $i = 1, 2, \dots, N$. Here, N is the number of electrons and K is the number of states generated by the electronic basis set. These molecular spin orbitals, ϕ_j , are expressed as a linear combination of atomic (LCAO) spin orbitals formed from Gaussian functions centered on the average nuclear position, \mathbf{R}_k , of the dynamically moving nuclei with momentum \mathbf{P}_k through electron-translation factors [33]. The z_{ij} coefficients describe the probability amplitude for electronic excitations of the system into the $K - N$ unoccupied (excited) states. Forming the quantum-mechanical Lagrangian, in the limit of zero width nuclear wave functions (classical trajectories) and using the TDVP, produces a set of dynamical equations that govern the time evolution of the dynamical variables $\{z, \mathbf{R}, \mathbf{P}\}$. The simplest END approximation can be labeled time-dependent Hartree-Fock (TDHF) for electrons and narrow wave-packet nuclei. This approximation has been implemented in the EN-Dyne code [44], version 2.8, used in this work.

Once the wave function is determined at the end of the time evolution, the electron-excitation probability, as a function of time t and initial atom separation R_0 , is obtained by performing a projection of the atomic n th state as

$$P_n(t, R_0) = |\langle \Phi_n | \Psi(t, R_0) \rangle|^2, \quad (4)$$

where Φ_n is the final excited state of the Li atom and Ψ is the final evolved total wave function.

For the purpose of discussing charge exchange during the dipole interaction, we introduce the Mulliken charge population approach [45–48]. This procedure allows one to partition the electron density in a multinuclear system and associate a probability of the electron population with each center to estimate partial atomic charges. The charge of the fragment is then the difference between the nuclear charge associated with the fragment and its computed probabilistic electron population. In the Mulliken scheme [45–47] for partitioning the system charge among the participating nuclei, each electron in the system is described by a spin orbital given by Eq. (3), such that the total electron charge density becomes

$$\rho = \sum_{\text{spin}} \sum_{\kappa, \lambda} \sum_{i=1}^N z_{\kappa i} z_{\lambda i}^* \phi_{\kappa} \phi_{\lambda}^*. \quad (5)$$

Integration of the charge density over all space yields the number of electrons

$$N = \sum_A n_A, \quad (6)$$

where the electron population on atom A is defined as

$$n_A = \sum_{\kappa, \lambda \in A} \sum_{i=1}^N z_{\kappa i} z_{\lambda i}^* \mathcal{S}_{\lambda \kappa}, \quad (7)$$

with the overlap integrals $\mathcal{S}_{\lambda \kappa} = \langle \phi_{\lambda} | \phi_{\kappa} \rangle$ defined in terms of ϕ_{κ} , i.e., a LCAO that constitute the molecular orbital. This is a good measure of the electronic atomic charge (probability) when the atoms are far apart, but less meaningful when they strongly interact as this definition divides the overlap contributions equally between the two atoms involved.

Following Mulliken interpretation, each fragment carries a probability charge, with a probabilistic interpretation of fractional charges in accord with quantum mechanics [45–49]. Thus, in an experimental measure, the fractional charge of an atom would mean that, in average, it will come out neutral with that probability and the remaining probability as an ion. In order to have a good physical meaning of the Mulliken charge population, the basis set used in each atom must be “balanced.” Basis sets are considered balanced when they include both polarization and diffuse functions in every atom center with the same proportion [50].

In the END approach, the equations of motion [33] for the nuclei are given by

$$\begin{aligned} i(\mathbf{C}_R \dot{\mathbf{z}} - \mathbf{C}_R^T \dot{\mathbf{z}}^*) + \mathbf{C}_{RR} \dot{\mathbf{R}} + (\mathbf{C}_{RP} - \mathbf{I}) \dot{\mathbf{P}} &= \nabla_{\mathbf{R}} E, \\ i(\mathbf{C}_P \dot{\mathbf{z}} - \mathbf{C}_P^T \dot{\mathbf{z}}^*) + (\mathbf{I} + \mathbf{C}_{RP}) \dot{\mathbf{R}} + \mathbf{C}_{PP} \dot{\mathbf{P}} &= \nabla_{\mathbf{P}} E, \\ -i\mathbf{C}_z \dot{\mathbf{z}} - i\mathbf{C}_R^* \dot{\mathbf{R}} + i\mathbf{C}_P \dot{\mathbf{P}} &= \nabla_{\mathbf{z}} E, \end{aligned} \quad (8)$$

where $\nabla_{\mathbf{y}} E = \partial E / \partial \mathbf{y}$ is the gradient (force) by the variable \mathbf{y} , $\dot{\mathbf{z}} = d\mathbf{z}/dt$ determines the nonadiabatic electronic transitions rate, and $E = \sum_l P_l^2 / 2M_l + \langle z, \mathbf{R}, \mathbf{P} | H_{el} | z, \mathbf{R}, \mathbf{P} \rangle$ is the total energy of the system, with M_l the nuclear mass and H_{el} the electronic Hamiltonian which includes the nuclear-nuclear repulsion term. The nonadiabatic coupling matrix terms

between electrons and nuclei are expressed as

$$C_{ph;qg} = \frac{\partial^2 \ln S}{\partial z_{ph}^* \partial z_{qg}} \Big|_{R'=R, P'=P},$$

$$(C_{X_{ik}})_{ph} = \frac{\partial^2 \ln S}{\partial z_{ph}^* \partial X_{ik}} \Big|_{R'=R, P'=P},$$

$$(C_{XY})_{ij;kl} = -2 \operatorname{Im} \frac{\partial^2 \ln S}{\partial X_{ij} \partial Y_{kl}} \Big|_{R'=R, P'=P},$$

which are defined in terms of the overlap $S = \langle z, \mathbf{R}, \mathbf{P} | z, \mathbf{R}', \mathbf{P}' \rangle$ of the determinantal states of two different nuclear configurations. Consequently, there are average forces that act on each nuclei produced by the excitations, the coupling between the electrons and the nuclei position, and the momentum; all these produce a nonadiabatic dynamics. Thus the dynamic is not only induced by Newton's forces from the Coulombic interactions but rather from a richer quantum description from the coupling of electrons and nuclei. In particular, from Eq. (8), one notices that the final nuclei momentum is affected by the coupling of the electrons and nuclei. As the atom has a probability to be in either neutral or a charged state, the final kinetic energy is the average among these charge states in a single determinant description. From the final momentum of the atoms, we calculate its final kinetic energy (KE).

C. Computational details

For the study of the dipole-induced process of a HeH^+ molecular ion in the neighborhood of an excited $\text{Li}(2p)$ atom, we require the specification of initial conditions of the system under consideration. Initially, a $\text{Li}(1s^2 2p)$ atom (system A) is placed on the z axis at an initial distance R_0 from system B, which consists of a $\text{HeH}^+(1\sigma_g^2)$ molecular ion whose center of mass is placed at the origin. The strongest dipole interaction occurs when the HeH^+ molecule bond is aligned along the direction of the Li atom. The atoms' centers are placed on the z axis, with both of them having zero initial momentum (initially at rest). In Fig. 1, we show a sketch of the initial configuration of the system and how the VPD process takes place, depicting the different possible final channels. Notice that the $2s$ electron from atom A has been excited into the $2p$ to become the excited neighbor.

The electronic basis set used to describe the H, He, and Li atoms is the aug-cc-pVDZ basis set from Dunning [50]. For the case of the Li atom, the basis set includes two diffuse s and p even-tempered orbitals [51,52] to better describe the $2p$ excited state. This basis set provides a good compromise between computational time and a proper description of the system dynamics. The initial separation, R_0 , ranges from 8 to 24 a.u. in steps of 0.4 a.u. from 8 till 10, in steps of 1 a.u. from 11 till 20 a.u., and finally 24.0, which corresponds to a range from 4.5 to 13 Å. As we have a heteronuclear diatomic molecule, we place the lithium atom along the molecule axis on both sides of the molecule, i.e., facing the He atom or facing the H atom; thus the number of initial R_0 separations duplicates.

The dynamics is carried out in the following way. At a given initial separation R_0 of the system, the initial molecular wave function is constructed as a LCAO of the resulting SCF

procedure to generate the wave function for the $\text{HeH}^+(1\sigma_g^2)$ in a n -vibrational state (see below) and the $\text{Li}(2p)$. The nuclear motion starts at rest ($\mathbf{P}_i = 0$) such that the dipole interaction induces the dynamics. The set of Eqs. (8) is solved numerically through the ENDyne suit code to find the new set of \mathbf{z} , \mathbf{R} , and \mathbf{P} variables at any time. Equations (4) and (7) are used to obtain the probabilities for electronic transitions (excitation and deexcitation). Equations (8) determine the time-dependent trajectories (position and momentum of the nuclei). The results of these equations are shown in all the figures. The evolution is carried out until a final time of 10 ps (≈ 400000 a.u.) with an adaptive time step of 1×10^{-6} a.u. as the largest in order to maintain numerical accuracy. Each trajectory takes around 1 week in a 3 GHz computer.

In the case of system B, (HeH^+), we perform initially a vibrational sampling for initial conditions of the nuclei in phase space. As our intent is to study the effect of the initial vibrational state, we restrict our sampling to starting the dynamics at the classical turning points of the ground-state potential-energy curve (PEC), where the nuclei are initially at rest. In Fig. 2, the blue symbols are the results obtained for the HeH^+ ground-state energy at the HF level of theory within the END approach. As HeH^+ is well described by a Hartree-Fock approach, the PEC is well represented by a Morse potential which provides the vibrational levels for the molecule in the ground state. The Morse potential and the lowest vibrational levels are shown in Fig. 2(a). The solid purple line is the Morse function

$$V(r) = D_e(1 - e^{-(r-r_0)/a})^2. \quad (9)$$

Here D_e is the dissociation energy of the molecule and a is related to the vibrational frequency through

$$\nu_0 = \frac{a}{2\pi} \sqrt{\frac{2D_e}{\mu}}, \quad (10)$$

with μ the reduced mass of the diatomic molecule. The vibrational energy is given by

$$E_n = h\nu_0 \left(n + \frac{1}{2} \right) - \frac{[(n + \frac{1}{2})h\nu_0]^2}{4D_e}. \quad (11)$$

In our case, we consider initial vibrational conditions from $n = 0$ to $n = 9$ including the zero point energy. We consider the two classical turning points where initially the atoms are at rest, as stated previously. This gives us a total of 21 initial vibrational positions for each separation of the system A and B. With this, we have a total of 533 trajectories for the numerical analysis.

As shown in the sketch of Fig. 1, there is a probability to have a chemical rearrangement process after the VPD. In order to verify that our basis set describes properly the final fragments, in Figs. 2(b) and 2(c), we show the PEC and some low vibrational levels obtained with the same basis set as well as the Morse potential curves for the cases of LiH and LiHe molecules. The binding energy of the LiHe molecule is very small, but still large compared to its experimental value [53]. Furthermore, we find that the bond length of the LiHe is around 4.3 Å, which is smaller than the experimental data [53]. This is a consequence of the lack of a good description

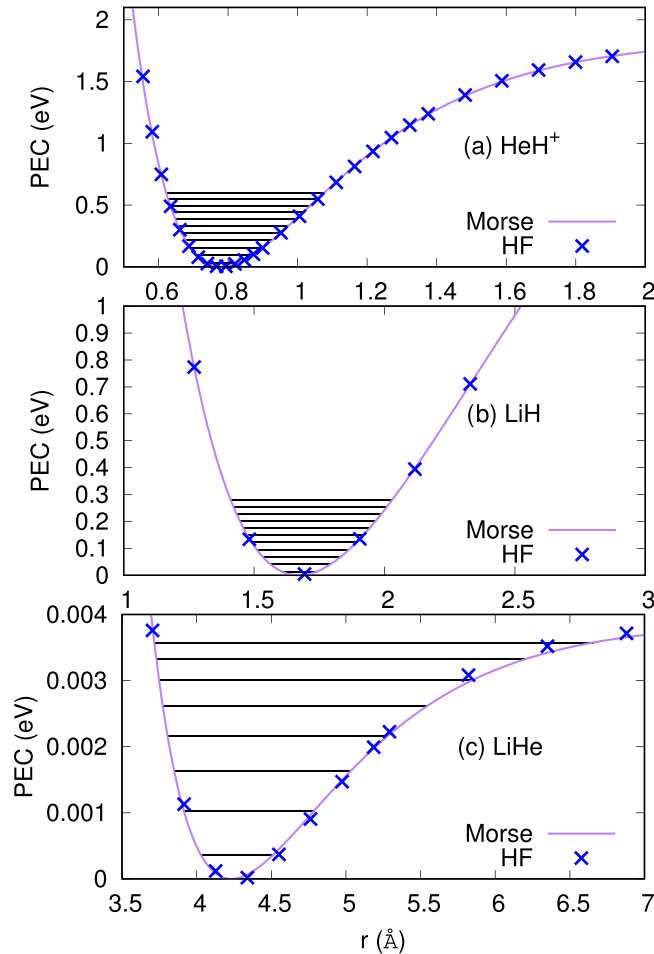


FIG. 2. Potential-energy curves (PECs) and vibrational energy levels of the three involved diatomic molecules. The blue crosses are the results of HF calculations and the purple solid lines are the respective Morse potentials, Eq. (9). The horizontal lines represent vibrational energy levels with the respective classical turning points. (a) HeH⁺, (b) LiH, and (c) LiHe. See text for discussion.

of electronic correlation for this weak molecular bond. In Table I, we provide the values for the PEC, as required by Eq. (9), obtained at the HF level with the END approach for reference purposes.

III. RESULTS

A. Dipole-induced processes

1. Trajectories and charge distribution

In Fig. 3(a), we show the time evolution of the atomic positions for the excited Li atom and the HeH⁺ ion in its

TABLE I. Values for D_e , a , and r_e , in a.u. as obtained at the HF level of theory within the END approach.

	LiH ⁺	LiH	LiHe
D_e	0.068 20	0.106 52	0.000 14
a	1.503 73	0.549 54	0.688 87
r_0	1.475 48	3.157 70	7.998 00

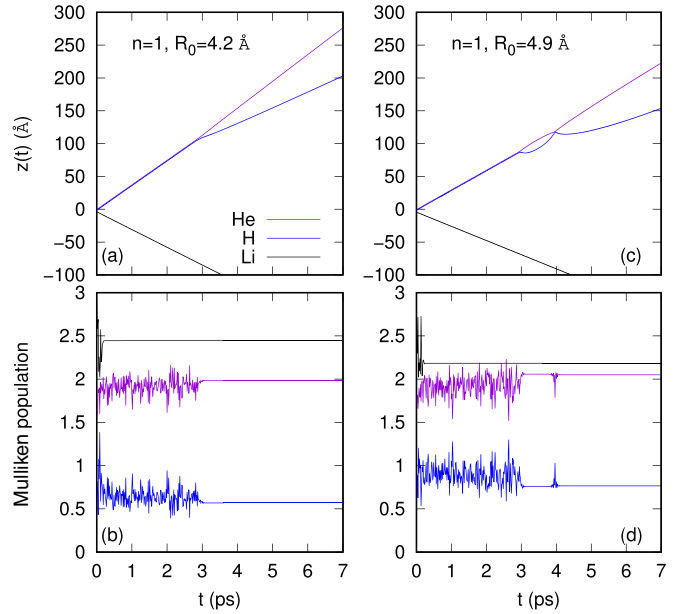


FIG. 3. Dipole-induced dissociation by an excited Li($2p$) atom near a HeH⁺ molecule. Frame (a) shows the position, $z(t)$, of the H, He, and Li atoms as a function of time, corresponding to an initial separation of $R_0 = 4.2$ Å in the initial vibrational state $n = 1$ of the HeH⁺ molecule as obtained from Eq. (8). The black dotted line corresponds to Li, the purple solid line to He, and the blue long-dashed line is for the hydrogen atom. In frame (b), we show the Mulliken population, according to Eq. (7), for each atom with the same line colors as in frame (a). In frame (c), we show the atoms' positions as a function of time for the case of an initial separation of $R_0 = 4.9$ Å and in the $n = 1$ vibrational state of the HeH⁺ molecule. In frame (d) we show the corresponding Mulliken population. See text for discussion.

$n = 1$ vibrational level for the case of an initial separation of $R_0 = 4.2$ Å, as a first example of a dipole-induced process for a low-vibrational state. The blue long-dashed line corresponds to the H atom position, the purple solid line to He, and the black dotted line to Li. These trajectories are obtained by solving the coupled Eqs. (8), as discussed previously. Note that, initially, there is a repulsion induced by the dipole interaction and then, around 3 ps, the HeH⁺ molecule dissociates, as observed in Fig. 3(a). In Fig. 3(b), we show the corresponding Mulliken charge population for each atom as a function of time as determined from Eqs. (7) and (8). Initially, we find that the $2p$ electron in the Li atom decays very fast (fs), partially to the $2s$ state but mostly a large fraction of it is deexcited (transferred) to the HeH⁺ molecule, with a 40% probability for the electron to remain in the Li atom, as obtained from Eq. (4). After dissociation, a neutral helium atom comes out, with 40% probability of having a neutral Li atom and 60% probability of having a neutral H atom. Let us recall that in the single determinant and the narrow wave packet of the nuclei, the other VPP have a null contribution for this initial condition. Thus a relaxation (deexcitation) of the $2p$ electron in the Li atom can occur into the neighbor molecule and induce dissociation.

Another example of a dipole-induced process is shown in Fig. 3(c), where the time dependence of the atoms

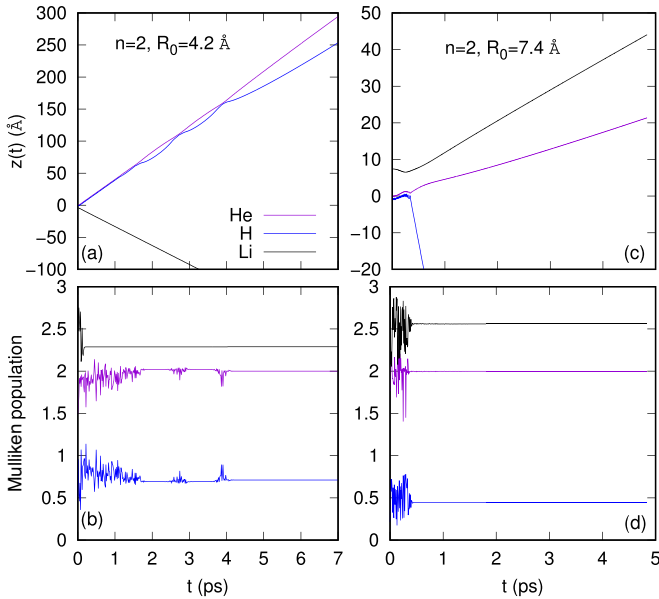


FIG. 4. Same as in Fig. 3, but for the initial separation of $R_0 = 4.2$ Å in (a) and $R_0 = 7.4$ Å in (c) for the initial vibrational state of $n = 2$ in both cases. In (a) the lithium atom is placed on the He side of the molecule, while in (b) it is placed on the H side. See text for discussion.

position, similar to Fig. 3(a), is presented, but for the case of an initial separation of $R_0 = 4.9$ Å with the HeH^+ initial vibrational level $n = 1$. The Mulliken population analysis, shown in Fig. 3(d), indicates that the HeH^+ molecule is neutralized with an 80% probability while the Li^+ ions leave the system via Coulomb repulsion. In both cases, one observes how the Mulliken charge population gets stabilized once the atoms are well separated. Notice that, in both Figs. 3(a) and 3(c), the Li atom is initially placed on the side of the hydrogen atom.

Similarly, in Fig. 4(a), we show the position of each of the atoms as a function of time, but now for an initial vibrational level $n = 2$ and at an initial distance between the Li atom and the center of mass of the HeH^+ molecule of $R_0 = 4.2$ Å when the Li atom is placed on the He side of the molecule. We observe that, after 1.8 ps in time, the HeH^+ system begins to dissociate via high vibrational excitations with the dissociation occurring around 4 ps. In Fig. 4(b), the Mulliken charge population analysis indicates that the electron in the $2p$ state partially decays into the $2s$ state of the lithium atom and a larger fraction is carried away by the H atom, with 70% probability, with the remaining 30% probability remaining in the Li ion. The He atom is released fully neutralized.

At a larger initial separation $R_0 = 7.4$ Å and $n = 2$, one observes an initial dipole attraction followed by dissociation of the molecule induced by the presence of the Li atom as shown in Fig. 4(c). However, the time for dissociation is shorter, 0.3 ps, and the velocity of the fragments is smaller. The initial $2p$ electron is transferred, during the dipole-induced process, to the H atom, as shown by the Mulliken charge population in Fig. 4(d), with a 45% probability.

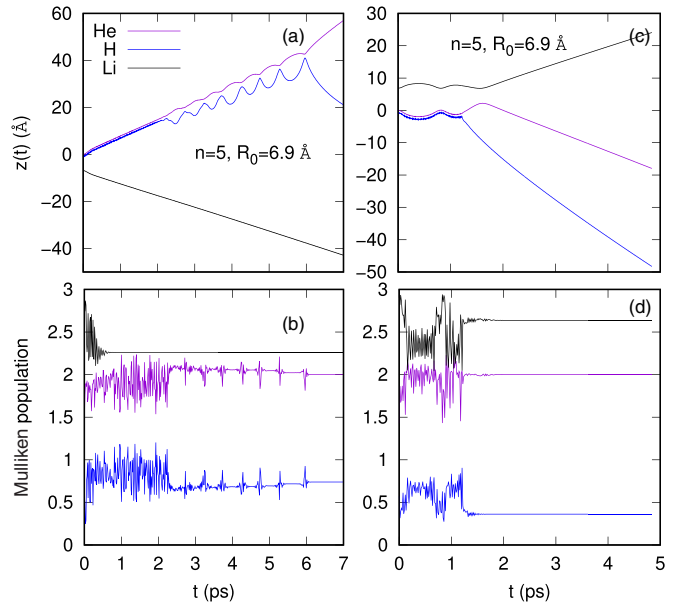


FIG. 5. Same as in Fig. 3, but for the initial separation of $R_0 = 6.9$ Å for the initial vibrational state $n = 5$ in both (a) and (c). In (a), the lithium atom faces the H atom of the HeH^+ molecule, while in (c) it faces the He atom. See text for discussion.

In Fig. 5, we show the dipole-induced process when the molecule is in a higher initial vibrational excited state, $n = 5$, and the system has an initial separation of $R_0 = 6.9$ Å. We observe charge transfer that neutralizes the HeH^+ molecule, followed by an increase in the vibrational excitation that occurs from 2 to 6 ps into a highly vibrational state, followed by dissociation. The hydrogen atom remains with a 75% electron probability of being neutral, as observed in Fig. 5(b). In Fig. 5(c), we show the VPD case for the same conditions as in Fig. 5(a), but when the Li atom is placed on the He side. In this case, we observe an initial vibration of the $\text{Li}+\text{HeH}^+$ whole system induced by van der Waals forces followed by the dissociation of HeH^+ .

By increasing further the initial vibrational state to $n = 9$ for an initial system separation of $R_0 = 10.6$ Å, we show the dipole process in Fig. 6(a). For the case of Fig. 6(a), we observe no VPD effect until a time around 4 ps. Then a slight repulsion occurs followed by an attraction at 5 ps with a subsequent dissociation of the HeH^+ molecule. In Fig. 6(c), we show the case for $R_0 = 4.7$ Å and observe that the deexcitation of the $2p$ electron induces a sudden repulsion consequence of the charge transfer of the $2p$ electron into the HeH molecule inducing a large vibrational state of the HeH^+ system that dissociates at 0.4 ps. Notice that the larger the separation of the Li atom to the HeH^+ molecule, the longer it takes for the electronic decaying process.

The dissociation of the HeH^+ molecule produces a neutral He atom and the release of a neutral or charged H depending on the probability of electron relaxation from the Li atom, as observed in all the previous cases. The dominant channel is the electron transfer induced by the dipole interaction, while the VPD process has a smaller probability given by the Li atom to remain neutral.

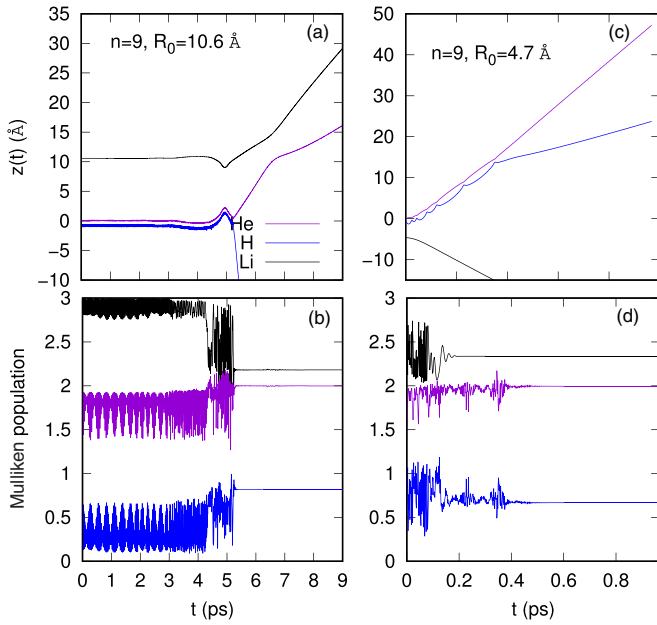


FIG. 6. Same as in Fig. 3, but for the initial separation of $R_0 = 10.9 \text{ Å}$ in (a) and $R_0 = 4.7 \text{ Å}$ in (c) for the initial vibrational state of $n = 9$. In (a) the Li atom faces the He atom, while in (c) it faces the H atom. See text for discussion.

2. Formation of LiHe and LiH

In Fig. 7, we show the dipole process that leads to the formation of LiHe⁺ and LiHe molecule for the cases of an initial separation of $R_0 = 7.9 \text{ Å}$ and initial vibrational state $n = 5$ in (a), as well as for the case $R_0 = 5.3$ and $n = 9$ in (c).

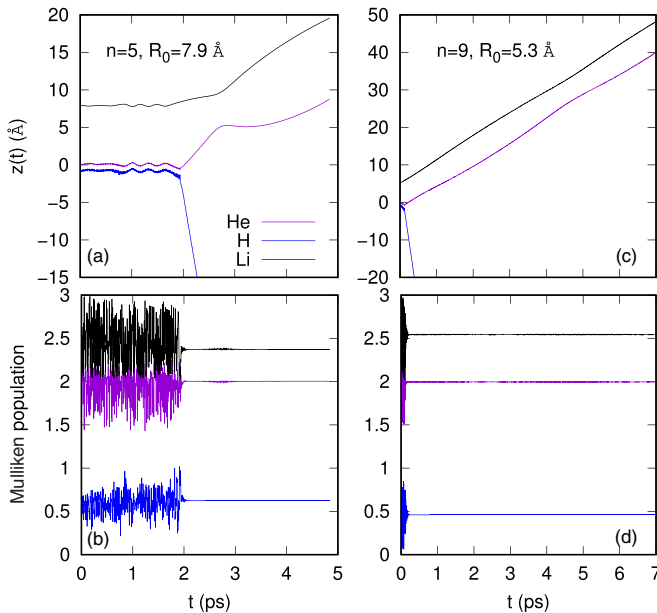


FIG. 7. LiHe formation via dipole-induced process for the initial separation of $R_0 = 7.9 \text{ Å}$ and $n = 5$ in (a) and $R_0 = 5.3 \text{ Å}$ for $n = 9$ in (c) for the process that leads to the formation of a LiHe molecule, as obtained from Eq. (8). In (b) and (d), we show the Mulliken charge population analysis, as obtained from Eq. (7). In both cases, the Li atom faces the He atom. See text for discussion.

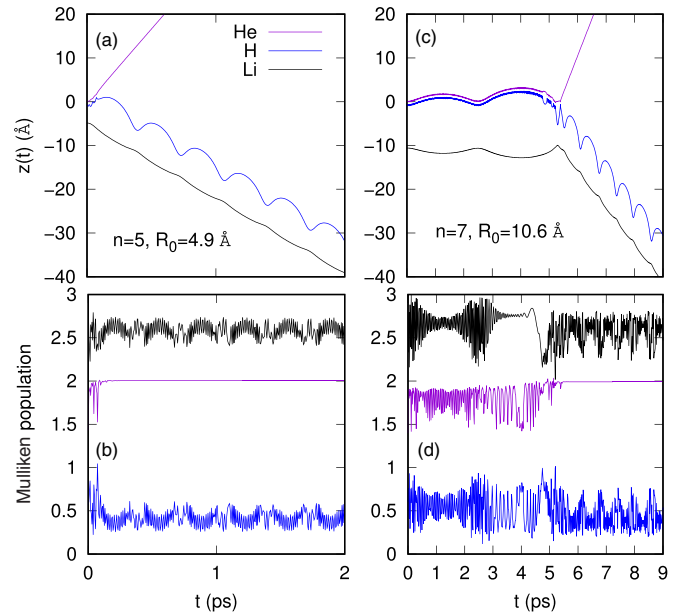


FIG. 8. LiH chemical rearrangement after dipole interaction of the HeH⁺ + Li(2p) system for the initial separation of 4.9 Å and $n = 5$ in (a) and 10.6 Å and $n = 7$ in (c). In (b) and (d), we show the Mulliken population analysis for each atomic center. See text for discussion.

In Fig. 7(a), we observe that the Li + HeH⁺ system interacts vibrationally via van der Waals forces until a time around 2 ps followed by the dissociation of the HeH⁺ molecule. As the Li atom is placed on the He side, it gets attracted and the formation of the LiHe molecule is likely. For the case shown in Fig. 7(c), we observe that, due to the higher initial excited state of the HeH⁺ molecule, the dipole interaction occurs much faster, around 0.2 ps, with the subsequent formation of the LiHe molecule. Thus the LiH molecule forms in an excited vibrational state with a large bond length.

The other likely outcome of the dipole interaction is the formation of LiH either neutral or charged, which has a higher probability of occurring when compared to the LiHe process. In Fig. 8(a), we show the formation of LiH for the cases where initially the HeH⁺ molecule is in the initial vibrational state $n = 5$ and placed at a distance of $R_0 = 4.9 \text{ Å}$ from the excited Li atom, as shown in (a). We find that the dynamics occurs very fast at around 0.1 ps with the release of a neutral He atom and the formation of a vibrationally excited LiH ion. The Mulliken population indicates that 60% probability of LiH outcomes are neutral, while a 40% probability are LiH⁺. By contrast, in Fig. 8(c), we show the same process resulting from a slower dynamics. Here, we show the case for $n = 7$ and $R_0 = 10.6 \text{ Å}$, finding that there is a dipole interaction between the Li atom and the HeH⁺ molecule driven by a charge exchange between the system up to a time around 5 ps. Afterwards a release of a neutral He atom follows, induced by the VPP with the formation of a higher vibrational LiH molecule, as observed from the Mulliken population analysis in Fig. 8(d). The He atom is released fully neutralized.

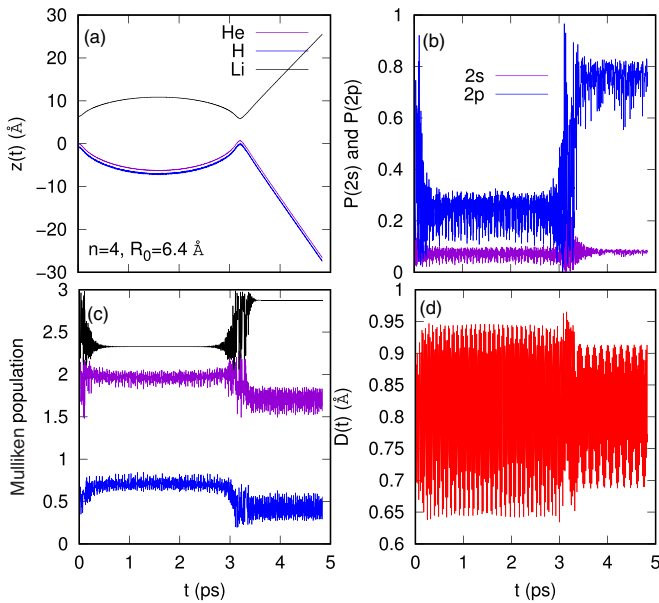


FIG. 9. Vibrational interatomic energy transfer for the case of an initial separation of $R_0 = 6.4 \text{ \AA}$ and $n = 4$. In (a), we show the trajectory of each atomic center. In (b), the probability of finding the valence electron in the $2s$ or $2p$ state. In (c), the Mulliken charge population analysis for each atomic center and, in (d), the HeH internuclear distance as a function of time showing the change in the vibrational amplitude. See text for discussion.

3. Vibrational intermolecular energy transfer

Recently, one of the authors [15] has shown that a neighbor system could induce energy transfer from vibrations, which is another dipole-induced process. In Fig. 9, we show that, for the case of $n = 4$ and an initial separation of $R_0 = 6.4 \text{ \AA}$, charge transfer occurs between the Li atom and the HeH^+ molecular ion with a subsequent Coulomb repulsion and vibrational relaxation. This process is induced by a decay of the $2p$ into the $2s$ state down to 20% probability in the first 0.1 ps, as shown in Fig. 9(b), where the probability of finding the valence electron of the Li atom in the $2s$ or $2p$ state is shown. The rest of the charge is transferred to the HeH^+ system, as shown in Fig. 9(c) where the Mulliken charge population is presented. However, at around 3 ps, the system reaches the closest distance, which is followed by a Coulomb repulsion. This process is caused by the vibrational energy relaxation of the system, as shown in Fig. 9(d), where the bond distance of the HeH molecule is shown. As the electron is transferred from the HeH back to the Li atom, the HeH molecule decreases its vibrational energy.

In Fig. 10, we show the case where only electronic decay is responsible for the vibrational internuclear energy transfer. This occurs for the case of $n = 3$ and $R_0 = 7.4 \text{ \AA}$ as shown in Fig. 10(a). One observes that the decay occurs in the first 0.1 ps for the $2p$ electron into the $2s$ state down to 20% probability, as shown in Fig. 10(b). In Fig. 10(c), we present the Mulliken charge population indicating that the Li charge remains almost the same. During the same time, we observe that the HeH^+ molecule increases its vibrational state, as shown in Fig. 10(d). At a time around 0.2 ps, the system repels the consequence of the electron returning back to its $2p$ state

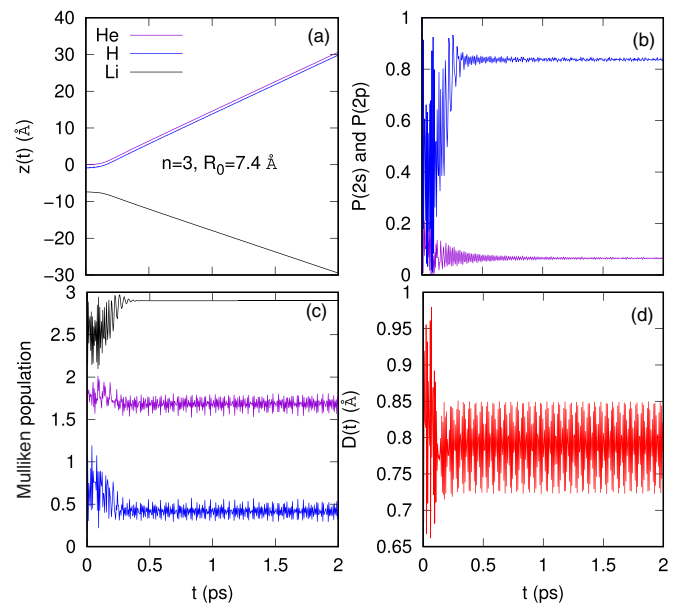


FIG. 10. Vibrational internuclear energy transfer for the initial separation of $R_0 = 7.4 \text{ \AA}$ and $n = 3$ in (a). In (b), we show the probability to find an electron in the initial $2p$ state and final $2s$ state of the lithium atom. In (c), we show the Mulliken charge population and in (d) we show the distance between the He and H atom to see the vibration evolution of the HeH^+ molecule. See text for discussion.

driven by the relaxation of the vibrational state in the HeH^+ molecule.

In Fig. 11, we show the case with the same initial conditions, as in Fig. 10, but now the Li atom facing the He atom. In this case, we observe that there is a Coulombic repulsion that starts in the first fs, caused by an electronic decay of the $2p$ state into the $2s$ state but largely produced by an electron transfer to the HeH^+ system. The Li atom has

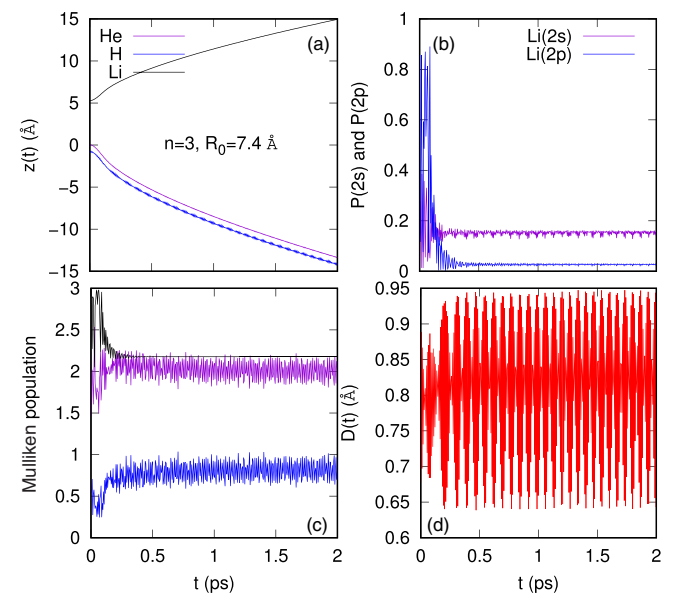


FIG. 11. Same as in Fig. 9, but for the initial separation of 7.4 \AA and $n = 3$. See text for discussion.

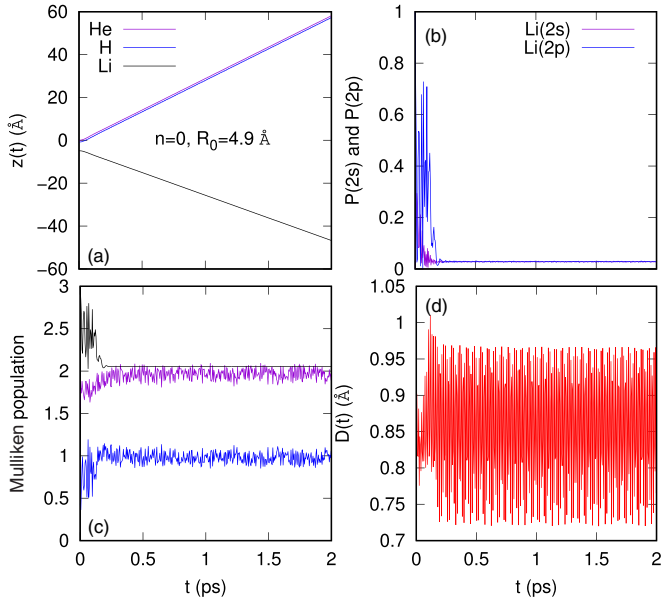


FIG. 12. Same as in Fig. 9, but for the initial separation of 4.9 Å and $n = 0$. See text for discussion.

a 20% probability to remain in the $2s$ state but the remaining probability goes into forming a neutral HeH molecule, as observed in Fig. 11(b). In this case, the electron transfer causes an increase on the vibrational state of the HeH molecule as observed in Fig. 11(d). Consequently, charge transfer induces an increase in the vibrational energy in the HeH system and a Coulomb repulsion between the Li⁺ atom and the HeH molecule. This previous instance is confirmed in Fig. 12, where we show the case for $n = 0$ and an initial separation of $R_0 = 4.9$ Å when the Li atom faces the H atom. We observe an immediate Coulombic repulsion between the Li atom and the HeH⁺ molecular ion driven by the initial electronic decay of the $2p$ electron into the $2s$ state of Li and a large charge transfer into the HeH⁺ molecule. The Li atom has a 5% probability for the electron to be found in the $2s$ and $2p$ states as seen in Fig. 12(b). However, 95% probability is transferred to neutralize the HeH⁺ molecular ion, as shown in Fig. 12(c). In Fig. 12(d), we observe the increase of the vibrational excitation in the HeH molecule consequence of the energy transfer between the systems.

These results confirm the vibrational interatomic energy-transfer mechanism proposed by Cederbaum [15]. Furthermore, we conclude that the Li($2p$) + HeH⁺ dynamics is more complex resulting in several processes, e.g., charge transfer, VPD, and the vibrational internuclear energy-transfer process.

B. Fragments final kinetic energy (KE)

We study the final kinetic-energy distribution of the fragments to gain an insight on the dipole-induced processes. In Fig. 13, we show the fragments final kinetic energy as a function of the initial separation between the Li and HeH⁺ molecule and the initial vibrational state of the system (different symbols), as deduced from the momentum of the nuclei and electron from Eqs. (8). We observe that the largest kinetic energy of the fragments is found for initial separations be-

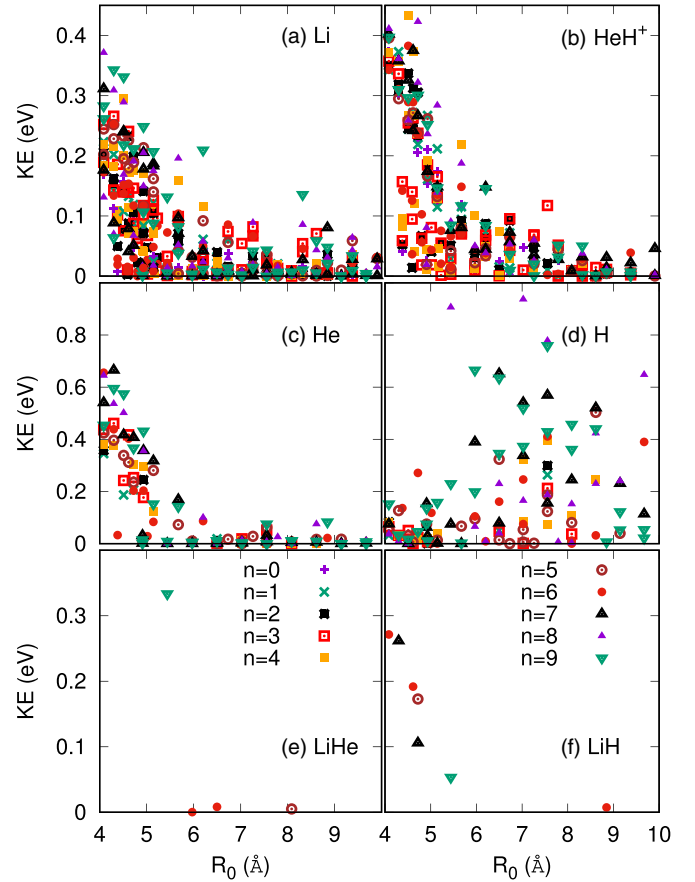


FIG. 13. Final kinetic energy (KE) of H, He, Li, LiH, and LiHe products resulting from the dipole-induced process, as a function of the initial separation between the Li and the HeH⁺ molecule. In (a), we show the KE for the Li atom, in (b) for HeH⁺, in (c) for the He atoms, in (d) for H atoms, in (e) for LiHe, and finally in (f) for the LiH molecule. See text for discussion.

tween 4 and 6 Å and up to 0.4 eV for the case of Li and HeH⁺ fragments. For the case of the He atom, we find a similar behavior but with a higher final kinetic energy, up to 0.8 eV for short distances. For the case of the H fragment, we find that all the initial distances contribute and the kinetic energy is scattered over the energy range lower than 1 eV for high vibrational excitation. We find that the less probable channels are the chemical rearrangement channels, which have a small range in R_0 with low KE < 0.3 eV.

The previous results are better understood when we plot the number of particles within a kinetic-energy range. In Fig. 14, we show the number of fragments within a kinetic-energy binning. The binning was carried out by assuming a Boltzmann distribution, as given by the vibrational levels in the HeH⁺ molecule and a $\Delta KE = 0.05$ eV. In this case the partition function, $Z = \sum_{n=0} e^{-E_n/k_B T}$, allows us to calculate the intensity or particle number within a given kinetic-energy range as

$$I(\text{KE}) = \frac{1}{Z} \sum_n N_n(\text{KE}) e^{-E_n/k_B T}, \quad (12)$$

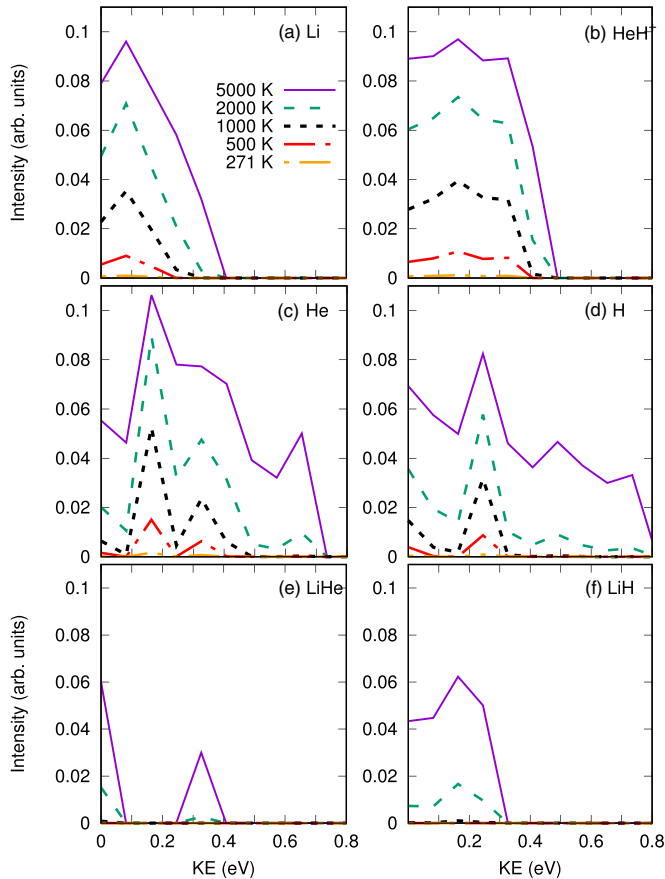


FIG. 14. Intensity of the final H, He, and Li products, as well as for LiH and LiHe, resulting from the dipole-induced process, as a function of the kinetic energy (KE) of the products in eV. In (a), we show the intensity for the Li atom, in (b) we show the intensity of HeH^+ , in (c) for the He atoms resulting from dissociation of HeH^+ , in (d) we report the intensity of the H atoms, in (e) for LiHe, and finally in (f) for the LiH molecule. See text for discussion.

where E_n is the initial vibrational energy of the HeH^+ molecule, $N_n(\text{KE})$ is the number of fragments within a kinetic-energy KE binning, and T is the vibrational temperature of the system.

Figure 14 shows that the Li and HeH fragments have the largest intensity but with a small kinetic energy (less than 0.4 eV), followed by the He and H fragments. As the He and H atoms are lighter than Li, their kinetic energy is higher, reaching up to 0.8 eV. Finally, the LiHe and LiH fragments have the smallest probability. The LiHe fragments show two peaks, one at 0.04 eV and the other at 0.32 eV, while the

LiH fragment is spread between 0 and 0.3 eV with a peak at 0.17 eV. Notice that the higher the temperature, the higher the contributions of all the fragments, as expected.

IV. CONCLUSIONS AND OUTLOOK

We studied the dipole-induced processes on a HeH^+ molecule in the neighborhood of an excited lithium atom as a function of time. The electronic structure of the system is carried out at the level of time-dependent Hartree-Fock by means of the electron-nuclear dynamics theory. Our results show that the $2p$ electron of the Li atom relaxes, starting to fill the $2s$ shell, while the excess energy is utilized to dissociate or recombine the chemical bond of the neighboring HeH^+ molecule via a virtual photon. In other cases, the $2p$ electron relaxes into the HeH^+ molecule or the H or He fragment. We find that the He atom is always released neutral. These processes are driven by a dipole-dipole interaction between the excited lithium atom and the molecule. Our results set an upper bound to the original picture of virtual photon exchange [30,54] dominated by charge transfer. We show that the VPD process is a particular case of the dipole interaction between neighbors induced by a virtual photon process (VPP). We find that high vibrational energy levels contribute with a large probability for dissociation, chemical rearrangement, and vibrational interatomic energy transfer. Thus the present version of the END approach provides an interesting and rich physical description of the processes driven by dipole-dipole interaction by taking into account the time evolution and the electron-nuclei coupling. For the HeH^+ , a single determinant describes properly the dissociation process, the fingerprints of which can be seen in the results. For a better description of these processes, a multiconfigurational description of the electronic structure and quantum wave-packet dynamics for the nuclei are required. Work is in progress to incorporate them into the framework of END.

In conclusion, we have shown that dipole interactions through virtual photon processes produce a richer dynamics in the femto- to picosecond scale. We hope our theoretical results will motivate further theoretical and experimental work to confirm our findings.

ACKNOWLEDGMENTS

R.C.-T. acknowledges support from grants UNAM-DGAPA-PAPIIT IN-111-820 and thanks the University of Heidelberg for its hospitality during the initial stages of this work. L.S.C. gratefully acknowledges financial support by the European Research Council (ERC) (Advanced Investigator Grant No. 692657).

[1] D. Comparat and P. Pillet, *J. Opt. Soc. Am. B* **27**, A208 (2010).
 [2] T. Förster, *Ann. Phys. (NY)* **437**, 55 (1948).
 [3] G. Scholes, G. Fleming, A. Olaya-Castro, and R. van Grondelle, *Nat. Chem.* **3**, 763 (2011).
 [4] L. S. Cederbaum, J. Zobeley, and F. Tarantelli, *Phys. Rev. Lett.* **79**, 4778 (1997).

[5] N. Sisourat, N. Kryzhevoi, P. Kolorenč, S. Scheit, T. Jahnke, and L. S. Cederbaum, *Nat. Phys.* **6**, 508 (2010).
 [6] R. Santra and L. S. Cederbaum, *Phys. Rep.* **368**, 1 (2002).
 [7] K. Gokhberg, P. Kolorenč, A. Kuleff, and L. S. Cederbaum, *Nature (London)* **505**, 661 (2014).
 [8] F. Trinter, M. Schöffler, H. Kim, F. P. Sturm, K. Cole, N. Neumann, A. Vredenburg, J. Williams, I. Bocharova,

- R. Guillemin, M. Simon, A. Belkacem, A. L. Landers, T. Weber, H. Schmidt-Böcking, R. Dörner, and T. Jahnke, *Nature (London)* **505**, 664 (2014).
- [9] P. O’Keeffe, E. Ripani, P. Bolognesi, M. Coreno, M. Devetta, C. Callegari, M. Di Fraia, K. C. Prince, R. Richter, M. Alagia, A. Kivimäki, and L. Avaldi, *J. Phys. Chem. Lett.* **4**, 1797 (2013).
- [10] M. Kimura, H. Fukuzawa, T. Tachibana, Y. Ito, S. Mondal, M. Okunishi, M. Schöffler, J. Williams, Y. Jiang, Y. Tamenori, N. Saito, and K. Ueda, *J. Phys. Chem. Lett.* **4**, 1838 (2013).
- [11] I. Cherkas and N. Moiseyev, *Phys. Rev. B* **83**, 113303 (2011).
- [12] A. Bande, K. Gokhberg, and L. S. Cederbaum, *J. Chem. Phys.* **135**, 144112 (2011).
- [13] A. Haller, D. Peláez, and A. Bande, *J. Phys. Chem. C* **123**, 14754 (2019).
- [14] H. Agueny, M. Pesche, B. Lutet-Toti, T. Miteva, A. Molle, J. Caillat, and N. Sisourat, *Phys. Rev. B* **101**, 195431 (2020).
- [15] L. S. Cederbaum, *Phys. Rev. Lett.* **121**, 223001 (2018).
- [16] E. F. van Dishoeck and R. Visser, Molecular photodissociation, in *Laboratory Astrochemistry: From Molecules through Nanoparticles to Grains*, edited by S. Schlemmer, T. Giesen, and H. Mutschke (Wiley, New York, 2015), Chap. 4.
- [17] A. N. Heays, A. D. Bosman, and E. F. van Dishoeck, *Astronomy & Astrophysics* **602**, A105 (2017).
- [18] V. Averbukh and L. S. Cederbaum, *J. Chem. Phys.* **123**, 204107 (2005).
- [19] S. Kopelke, K. Gokhberg, V. Averbukh, F. Tarantelli, and L. S. Cederbaum, *J. Chem. Phys.* **134**, 094107 (2011).
- [20] N. Moiseyev, *Isr. J. Chem.* **31**, 311 (1991).
- [21] M. K. Mishra and M. N. Medikeri, Characterization of shape and Auger resonances using the dilated one electron propagator method, *Advances in Quantum Chemistry* (Academic Press, New York, 1996), Vol. 27, pp. 223–295.
- [22] R. Santra, L. Cederbaum, and H.-D. Meyer, *Chem. Phys. Lett.* **303**, 413 (1999).
- [23] N. Vaval and L. S. Cederbaum, *J. Chem. Phys.* **126**, 164110 (2007).
- [24] A. Ghosh, S. Pal, and N. Vaval, *Mol. Phys.* **112**, 669 (2014).
- [25] R. Santra, J. Zobeley, L. S. Cederbaum, and N. Moiseyev, *Phys. Rev. Lett.* **85**, 4490 (2000).
- [26] A. Landau, A. Ben-Asher, K. Gokhberg, L. S. Cederbaum, and N. Moiseyev, *J. Chem. Phys.* **152**, 184303 (2020).
- [27] G. Jabbari, K. Sadri, L. S. Cederbaum, and K. Gokhberg, *J. Chem. Phys.* **144**, 164307 (2016).
- [28] M. Shapiro and R. Bersohn, *Annu. Rev. Phys. Chem.* **33**, 409 (1982).
- [29] G. G. Balint-Kurti, R. N. Dixon, and C. C. Marston, *J. Chem. Soc., Faraday Trans.* **86**, 1741 (1990).
- [30] L. S. Cederbaum, *J. Phys. Chem. Lett.* **11**, 8964 (2020).
- [31] R. Güsten, H. Wiesemeyer, D. Neufeld, K. M. Menten, U. U. Graf, K. Jacobs, B. Klein, O. Ricken, C. Risacher, and J. Stutzki, *Nature (London)* **568**, 357 (2019).
- [32] I. Dumitriu and A. Saenz, *J. Phys. B: At., Mol., Opt. Phys.* **42**, 165101 (2009).
- [33] E. Deumens, A. Diz, R. Longo, and Y. Öhrn, *Rev. Mod. Phys.* **66**, 917 (1994).
- [34] R. Cabrera-Trujillo, J. R. Sabin, Y. Öhrn, and E. Deumens, *Phys. Rev. A* **61**, 032719 (2000).
- [35] R. Cabrera-Trujillo, J. R. Sabin, Y. Öhrn, and E. Deumens, *Phys. Rev. Lett.* **84**, 5300 (2000).
- [36] N. Stolterfoht, R. Cabrera-Trujillo, Y. Öhrn, E. Deumens, R. Hoekstra, and J. R. Sabin, *Phys. Rev. Lett.* **99**, 103201 (2007).
- [37] R. Cabrera-Trujillo, Y. Öhrn, E. Deumens, and J. R. Sabin, *J. Chem. Phys.* **116**, 2783 (2002).
- [38] B. J. Killian, R. Cabrera-Trujillo, E. Deumens, and Y. Öhrn, *J. Phys. B: At., Mol., Opt. Phys.* **37**, 4733 (2004).
- [39] R. Cabrera-Trujillo, E. Deumens, Y. Öhrn, O. Quinet, J. R. Sabin, and N. Stolterfoht, *Phys. Rev. A* **75**, 052702 (2007).
- [40] R. Cabrera-Trujillo, Y. Öhrn, E. Deumens, and J. R. Sabin, *J. Phys. Chem. A* **108**, 8935 (2004).
- [41] R. Cabrera-Trujillo, Y. Öhrn, E. Deumens, J. R. Sabin, and B. G. Lindsay, *Phys. Rev. A* **70**, 042705 (2004).
- [42] R. Cabrera-Trujillo, *Phys. Rev. A* **103**, 032812 (2021).
- [43] R. Cabrera-Trujillo, O. Vendrell, and L. S. Cederbaum, *Phys. Rev. A* **102**, 032820 (2020).
- [44] E. Deumens, T. Helgaker, A. Diz, H. Taylor, J. Oreiro, B. Mogensen, J. A. Morales, M. C. Neto, R. Cabrera-Trujillo, and D. Jacquemin, *ENDyne version 2.8 Software for Electron Nuclear Dynamics*, Quantum Theory Project, University of Florida, Gainesville, FL 32611-8435, 2000.
- [45] R. S. Mulliken, *J. Chem. Phys.* **23**, 1833 (1955).
- [46] R. S. Mulliken, *J. Chem. Phys.* **23**, 1841 (1955).
- [47] R. S. Mulliken, *J. Chem. Phys.* **36**, 3428 (1962).
- [48] R. Cabrera-Trujillo, Y. Öhrn, E. Deumens, and J. R. Sabin, *Phys. Rev. A* **62**, 052714 (2000).
- [49] C. T. Sebens, *Found. Phys.* **51**, 75 (2021).
- [50] T. H. Dunning, *J. Chem. Phys.* **90**, 1007 (1989).
- [51] R. C. Raffanetti, *J. Chem. Phys.* **59**, 5936 (1973).
- [52] R. D. Bardo, Master’s thesis, Iowa State University, Retrospective Theses and Dissertations, 1973.
- [53] N. Tariq, N. A. Taisan, V. Singh, and J. D. Weinstein, *Phys. Rev. Lett.* **110**, 153201 (2013).
- [54] V. Averbukh, I. B. Müller, and L. S. Cederbaum, *Phys. Rev. Lett.* **93**, 263002 (2004).